

RESEARCH ARTICLE | DECEMBER 10 2024

On the increase of the melting temperature of water confined in one-dimensional nano-cavities

Flaviano Della Pia ; Andrea Zen ; Venkat Kapil  ; Fabian L. Thiemann ; Dario Alfè ; Angelos Michaelides  



J. Chem. Phys. 161, 224706 (2024)
<https://doi.org/10.1063/5.0239452>



View
Online



Export
Citation

Articles You May Be Interested In

DMC-ICE13 : Ambient and high pressure polymorphs of ice from diffusion Monte Carlo and density functional theory

J. Chem. Phys. (October 2022)

Accurate nuclear quantum statistics on machine-learned classical effective potentials

J. Chem. Phys. (October 2024)

The wetting of H₂O by CO₂

J. Chem. Phys. (August 2024)



The Journal of Chemical Physics

Special Topics Open for Submissions

[Learn More](#)

On the increase of the melting temperature of water confined in one-dimensional nano-cavities

Cite as: J. Chem. Phys. 161, 224706 (2024); doi: 10.1063/5.0239452

Submitted: 19 September 2024 • Accepted: 21 November 2024 •

Published Online: 10 December 2024



View Online



Export Citation



CrossMark

Flaviano Della Pia,¹ Andrea Zen,^{2,3} Venkat Kapil,^{1,4,5,6,a)} Fabian L. Thiemann,⁷ Dario Alfè,^{2,3,5,6}
and Angelos Michaelides^{1,a)}

AFFILIATIONS

¹Yusuf Hamied Department of Chemistry, University of Cambridge, Cambridge CB2 1EW, United Kingdom

²Dipartimento di Fisica Ettore Pancini, Università di Napoli Federico II, Monte S. Angelo, I-80126 Napoli, Italy

³Department of Earth Sciences, University College London, London WC1E 6BT, United Kingdom

⁴Department of Physics and Astronomy, University College London, London, United Kingdom

⁵Thomas Young Centre, University College London, London WC1E 6BT, United Kingdom

⁶London Centre for Nanotechnology, University College London, London WC1E 6BT, United Kingdom

⁷IBM Research Europe, Keckwick Lane, Daresbury WA4 4AD, United Kingdom

^{a)}Authors to whom correspondence should be addressed: v.kapil@ucl.ac.uk and am452@cam.ac.uk

ABSTRACT

Water confined in nanoscale cavities plays a crucial role in everyday phenomena in geology and biology, as well as technological applications at the water–energy nexus. However, even understanding the basic properties of nano-confined water is extremely challenging for theory, simulations, and experiments. In particular, determining the melting temperature of quasi-one-dimensional ice polymorphs confined in carbon nanotubes has proven to be an exceptionally difficult task, with previous experimental and classical simulation approaches reporting values ranging from ~180 K up to ~450 K at ambient pressure. In this work, we use a machine learning potential that delivers first principles accuracy (trained to the density functional theory approximation revPBE0-D3) to study the phase diagram of water for confinement diameters $9.5 < d < 12.5$ Å. We find that several distinct ice polymorphs melt in a surprisingly narrow range between ~280 and ~310 K, with a melting mechanism that depends on the nanotube diameter. These results shed new light on the melting of ice in one-dimension and have implications for the operating conditions of carbon-based filtration and desalination devices.

© 2024 Author(s). All article content, except where otherwise noted, is licensed under a Creative Commons Attribution (CC BY) license (<https://creativecommons.org/licenses/by/4.0/>). <https://doi.org/10.1063/5.0239452>

I. INTRODUCTION

Water under nanometric confinement is ubiquitous in nature and important for chemistry, physics, biology, geology, and engineering. It has received attention from both experiments and theory. Experiments suggest anomalous properties such as low dielectric response,¹ anomalously soft dynamics with pliable hydrogen bonds,² and massive radius-dependent flow.³ Theory and simulations indicate quantum mechanically induced friction,^{4,5} ice–liquid oscillations,⁶ and possible superionic behavior.⁷ In addition to its potential for the discovery of new physics of confined liquids, nano-confined water has many promising applications, e.g.,

desalination⁸ and clean energy.^{9,10} In particular, water confined in carbon nanotubes (CNTs) has been of interest for quasi-one-dimensional phase transitions,^{11,12} macroscopically ordered water structures,¹³ a transition from Fickian to ballistic diffusion,^{14,15} ultra-fast water hydrodynamics,^{2,16–18} the formation of close-packed ice,¹⁹ as well as promising applications ranging from water purification to blue energy harvesting.^{20,21}

Both experiments^{22,23} and simulations^{11,18,24} suggest that the phase diagram of water confined in sub-nanometer tubes is significantly different from bulk water, with the formation of both ordered hollow and filled one-dimensional polymorphs, namely, ice nanotubes. Water confined in CNTs is of strong technological

interest in both solid and fluid phases. Ice nanotubes have potential applications for ferroelectric devices,^{25,26} while liquid water in CNTs is important for the development of high-flux membranes²⁷ and flow sensors²⁸ due to the strong analogy between CNTs and aquaporins^{29,30} and their potential to develop artificial water channels.³¹ In this context, it is important to ask in which temperature range water confined in nanotubes melts, with implications for all the aforementioned applications. The melting temperatures of ice nanotubes confined in CNTs have been an object of study in both simulations^{11,18,24} and experiments,^{22,32,33} especially below a critical confinement length scale (~ 2.5 nm), where the macroscopic Gibbs–Thomson relation predicts a depression of the freezing point of water, breaks down.^{34,35} However, measuring the melting temperature of water in narrow carbon nanotubes is a challenge both in experiments and simulations. In fact, x-ray diffraction (XRD) measurements^{22,23} reported melting temperatures ranging from ~ 300 K (pentagonal ice) to ~ 180 K (octagonal ice). These results are roughly in agreement with classical molecular dynamics (MD) simulations^{11,24} based on TIP4P³⁶ or SPC/E³⁷ water, as well as photoluminescence (PL) experiments.³² In contrast, Raman spectroscopy experiments³³ reported melting temperatures that were extremely sensitive to the CNT diameter, varying from ~ 450 K for $d \sim 10.5$ Å to ~ 280 K for $d \sim 15.2$ Å. Qualitatively similar results were subsequently obtained with ReaxFF³⁸ MD simulations in Ref. 18. In summary, the debate on the values of the melting temperature is still open: different experiments and (empirical force-field) simulations report values ranging from ~ 180 up to ~ 450 K. This seemingly basic disparity has large implications for the working conditions of liquid water and ice nanotubes in emerging nanotechnological applications. While different experimental techniques have been applied to investigate this problem, no computational work with the accuracy of electronic structure theory is available, mainly due to the significant length and timescale needed for reliable results.

In this work, we take a step toward computing the melting temperatures of one-dimensional nano-confined ice and understanding its ambient pressure phase diagram with predictive accuracy. In particular, we achieve first-principles accuracy with feasible computational cost by using a machine learning potential (MLP)^{39,40} trained on density functional theory (DFT) data (functional revPBE0-D3) and target the question: are room temperature ice nanotubes liquid in a one-dimensionally confined CNT-like cavity? To address this question, we study the melting temperature of nano-confined ice with an implicit model, i.e., by emulating the confining material with a cylindrical confining potential fitted to the water–carbon interaction in sub-nanometer carbon nanotubes. This is a standard approach in analyzing the phase behavior of quasi-one-dimensional nano-confined water,^{23,36,41} and we have checked the reliability of our implicit model toward the explicit modeling of the carbon atoms by using the MLP developed in Ref. 42. To compute the melting temperatures, we determine the most stable polymorphs for a fixed nanotube diameter by using random structure search (RSS)⁴³ and compute its melting temperature via solid–liquid coexistence simulations. We find the melting points of (helical) triangular, square, pentagonal, and hexagonal ice nanotubes to be ~ 10 – 30 K higher than the bulk water melting temperature. In addition, we report a non-monotonic behavior of the number of hydrogen bonds with the confining diameter that

positively correlates with the water diffusion coefficient. On the one hand, our results confirm the possibility of studying and applying ice nanotubes at around room temperature but suggest that the range of stability is limited at temperatures below ~ 310 K, as opposed to a previously higher suggested range. On the other hand, our results indicate that filtration and desalination devices based on water confined in narrow tubes do not require high working temperatures.

II. METHODS

To ensure both computational efficiency and accuracy, we follow a similar approach used in Ref. 7. We used: (1) a combination of available DMC and CCSD(T) data to select a DFT functional to describe the water–carbon interaction and parameterize a Morse potential, (2) an MLP trained on bulk and confined water structures for the water–water interaction,^{7,44} (3) random structure search (RSS) to identify metastable phases, and (4) solid–liquid coexistence simulations to compute the melting temperatures.

A. Separation of the potential energy surface

We split the potential energy of the system into the following: (1) water–CNT interaction, modeled using a radial confining potential fitted to DFT water–CNT binding energies; and (2) water–water interactions described by an MLP trained on DFT data. The water–CNT interaction is modeled with the revPBE-D3 functional, selected according to the benchmark on diffusion Monte Carlo (DMC) and Coupled Cluster with Single, Double, and perturbative Triple interactions [CCSD(T)] (previously computed in Ref. 45) data reported in Sec. S1 of the [supplementary material](#). The water–water interaction is modeled with the MLP trained on revPBE0-D3 data for bulk and confined water in Refs. 7 and 44. The MLP model relies on the Behler–Parrinello neural network framework³⁹ to form a committee neural network potential⁴⁶ and was trained with an active learning framework.⁴⁷ The DFT functional was selected based on DMC benchmarks,⁷ and the model has already been applied to the analysis of the phase diagram of monolayer confined water.^{7,44}

B. Structure search

We probe potential phases of ice nanotubes using the RSS approach in combination with the MLP. Within this approach, we recover the previously known ice polymorphs by optimizing a large set of structures generated by randomly placing water molecules within the confinement region at ambient pressure. The RSS is less suitable for the identification of helical structures, which require a specific number of molecules. We build helical ice nanotubes according to the theory described in Ref. 11 and optimize them with our model. The zero-temperature-zero-pressure stable phase is subsequently identified as the one with the lowest energy. The validity of our model has been tested toward DMC data for the CNT(15,0), as described in Sec. S3 of the [supplementary material](#).

C. Coexistence simulations

The melting temperatures of the confined ice nanotubes are determined via solid–liquid coexistence simulations. An initial solid

structure is thermalized at ~ 250 K; half of the oxygen is subsequently frozen, while the other half is melted at ~ 600 K and then quenched down to ~ 300 K. The interface between the solid and the liquid is built in the NVT ensemble to avoid large box fluctuations during the high-temperature melting phase. The coexistence simulations are subsequently run in the NP_zT ensemble with $P \sim 10$ bar and changing temperatures in the range of $\sim [250, 340]$ K.

The melting temperature is determined according to changes in the density and the diffusion coefficient as a function of temperature (which are plotted in Fig. 2). In particular, for $d \sim 9.5$ and ~ 10.2 Å, the density and diffusion coefficient as a function of the temperature present a discontinuity. With T_1 defined as the highest sampled temperature before the discontinuity and T_2 as the lowest sampled temperature after the discontinuity, the melting temperature is computed as $(T_1 + T_2)/2$. The error bar on the melting temperature is estimated as $(T_2 - T_1)/2$. For $d \sim 11.0, 11.8$, and ~ 12.5 Å, the density and diffusion coefficient present smoother behavior as a function of the temperature. In this case, we define T_1 as the largest sampled temperature for which the diffusion coefficient is $D_{zz} < 0.5 \times 10^{-9} \text{ m}^2 \text{ s}^{-1}$, and T_2 as the lowest sampled temperature for which $D_{zz} \sim 1 \times 10^{-9} \text{ m}^2 \text{ s}^{-1}$, comparable to the bulk water diffusion coefficient at room temperature. The melting temperature and its error bar are then estimated as above.

We note here that an alternative way to compute the melting temperature is via free energy calculations over cooling and heating ramps. However, for nano-confined ice, this approach requires longer time scales of hundreds of ns around the melting temperature,¹¹ and it is often affected by larger uncertainties due to the sensitivity to the heating and cooling rate. In addition, it has been shown that coexistence simulations provide a high precision strategy to determine the melting temperature of ice^{48,49} and that, in general, the phase coexistence and solid–liquid free energy approaches agree with the method's uncertainties.^{48–51}

Further technical details on the calculation of the density and the diffusion coefficient are reported in the following. The density is computed as the ratio of the number of molecules and the occupied volume inside the confining cylinder. To define the volume of the cylinder occupied by water molecules, we consider the radial density $\rho(r)$ as a function of the radial distance r . We define r_{max} as the maximum distance r such that $\rho(r) > 0$. The occupied volume V is computed as $V = \pi r_{\text{max}}^2 l_z$, where l_z is the length of the simulation box. The shaded error bars in Fig. 2(a) are computed considering a $\sim 5\%$ uncertainty in the definition of r_{max} . The diffusion coefficient of nano-confined ice is estimated using the VACF method. A comparative analysis of the estimate of the diffusion coefficient obtained by using the Einstein relation to extract the diffusion coefficient from the Mean Square Displacement (MSD)⁵² and VACF is reported in the supplementary material. The two approaches deliver results in close agreement, and the VACF approach was chosen to present results in the main paper as it delivers smaller sampling uncertainties. The diffusion coefficient of the bulk is computed with the MSD method using a cubic box of side $L = 24.84$ Å containing 512 water molecules and applying the temperature-dependent finite-size correction from Ref. 53.

D. Computational details

Molecular Dynamics (MD) simulations are performed using the i-PI⁵⁴ code with the n2p2-LAMMPS^{55,56} library to calculate

the MLP energies and forces and an ASE⁵⁷ driver for the radial confining potential. The time step is fixed to 0.5 fs, and pressure and temperature are controlled with the generalized Langevin equation (GLE) barostat–thermostat as implemented in i-PI. Complete details on the development of the used MLP are given in Ref. 44.

Coexistence simulations have been performed with supercells containing ~ 700 water molecules (~ 40 nm long nanotubes) to limit finite-size effects. Tests on the effect of the number of water molecules on the density and the diffusion coefficient are reported in the supplementary material (Sec. S7). In particular, we show that density in our simulations is converged compared to simulations with $\sim 10^4$ water molecules, which is comparable with the number of molecules expected in experiments with CNTs of length $\sim 1 \mu\text{m}$. The length of the MD simulations varies from 10 to 20 ns depending on when convergence is achieved, as shown in the supplementary material.

The water–CNT confining potential is fitted to revPBE-D3 binding energies computed with a $1 \times 1 \times 3$ k-point grid and ~ 9 Å long nanotubes. All calculations are run using VASP^{58–61} with a 1000 eV energy cutoff, fine FFT grids, and hard pseudopotentials. Further details on the construction of the confining potential are given in the supplementary material (Sec. S2).

The DMC calculations are performed using the CASINO⁶² package, using eCEPP⁶³ pseudopotentials with the determinant-locality approximations,⁶⁴ and taking into account errors due to finite system size^{65–67} and finite time step⁶⁸ (convergence shown in the supplementary material). This setup was also used to study bulk ice,⁶⁹ yielding results in excellent agreement with experiments.

III. RESULTS AND DISCUSSION

A. The melting temperature of quasi-one-dimensional nano-confined ice

Previous experimental and empirical force-field based computational work suggests that water confined in sub-nanometer nanotubes exhibits an interesting phase diagram, with different quasi-one-dimensional ice polymorphs stable in different diameter ranges.^{11,23,32} In this work, we explore the phase behavior of ice confined in narrow nanotubes, i.e., with a diameter $d \sim 10$ Å, at first principles accuracy. Therefore, we considered five confining cylinders corresponding to zigzag nanotubes CNT($n,0$) with $n = 12, 13, 14, 15, 16$. The diameters of the considered nanotubes are, respectively, $\sim 9.5, 10.2, 11.0, 11.8, 12.5$ Å. The diameters were selected to maximize the variability in the studied phase diagram. In fact, a different one-dimensional ice polymorph is expected to be the most stable polymorph for each confining diameter.¹¹

To explore the phase behavior of the ice nanotubes, we use an implicit confinement model. We first developed a uniform cylindrical confining potential fitted to revPBE-D3^{70,71} binding energies of a water molecule inside the CNT. The DFT functional for the water–carbon interaction was determined via an accurate benchmark to DMC and CCSD(T) data from Ref. 45. The water–water interaction is described by using the MLP from Ref. 44, trained on revPBE0-D3^{71,72} for treating water in bulk and under confinement.^{7,44} To find all the metastable phases in each

nanotube, we performed an RSS with a home-built Python code. Subsequently, we identified the most stable polymorph in each nanotube based on the minimization of the enthalpy and then computed its melting temperature via coexistence simulations. The reliability of our model in determining the lowest enthalpy structure has been checked against both revPBE0-D3 and DMC data, as reported in Sec. S3 of the [supplementary material](#). Further technical details on the RSS, the fitting of the confining potential, and the coexistence simulations are reported in Sec. II and in the [supplementary material](#), together with tests on the robustness of our model with respect to the modeling of explicit carbon (Sec. S6). Considering the weak impact of quantum nuclear motion on the melting temperature of bulk⁷³ and 2D nanoconfined water⁷ at ambient pressures, we restrict ourselves to a classical description of the nuclei.

The most stable phases identified with our approach in the five considered nanotubes are (helical) triangular ($d \sim 9.5$ Å), square ($d \sim 10.2$ Å), pentagonal ($d \sim 11.0$ and ~ 11.8 Å), and hexagonal ice ($d \sim 12.5$ Å). Front-view snapshots of the zero-temperature structures are reported in Fig. 1(a). We refer to the melting temperature–diameter phase diagram in Fig. 1(b). The first

principles accuracy melting points obtained in this work are reported with a blue triangle, red square, orange and dark green pentagon, and light green hexagon. We find that the melting temperatures of ice nanotubes are ~ 10 – 30 K above the melting temperature of bulk water, which is 270 ± 5 K for our model.⁷ In particular, the melting point of the square ice nanotube is in quantitative agreement with PL³² spectroscopy. A much higher transition temperature was reported with Raman spectroscopy at similar diameters.³³ However, Chiashi *et al.*³² argue that the high temperature reported in Ref. 33 could be related to the observation of the encapsulation process (the vapor–liquid phase transition). The melting temperature of pentagonal and hexagonal ice nanotubes is in near quantitative agreement with XRD^{22,23} and Raman³³ experiments, considering the large experimental error bars and uncertainties on the confining diameter.

It is not straightforward to compare our results to the melting temperatures predicted by empirical water models. In fact, the MLP melting temperatures of square, pentagonal, and hexagonal ice are ~ 20 – 30 K higher than TIP4P, while the MLP melting temperature of triangular ice is ~ 90 K higher than the TIP4P prediction. However, TIP4P predicts a bulk melting temperature of ~ 230 K.⁷⁴

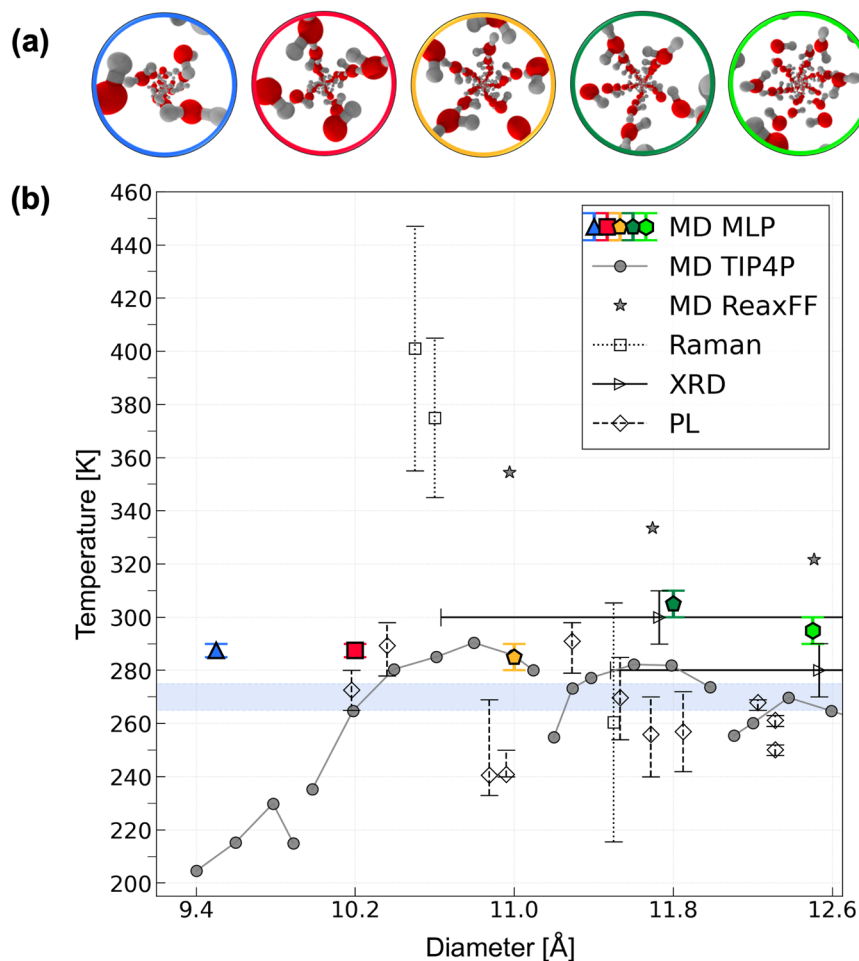


FIG. 1. Melting temperature of nanoconfined ice tubes. (a) Snapshots of the solid structures stable at zero temperature. Oxygen atoms are plotted in red, and hydrogen atoms are plotted in gray. (b) The melting temperatures of triangular (blue), square (red), pentagonal (orange and dark green), and hexagonal (light green) ice computed in this work are reported as a function of the confinement diameter. Empty black markers show the experimental results. In particular, we use diamonds with dashed error bars for PL,³² triangles with solid error bars for XRD,^{22,23} and squares with dotted error bars for Raman spectroscopy.³³ Previous empirical force-field MD simulations are reported with gray stars for results from Ref. 18 obtained with ReaxFF and gray circles for results from Ref. 11 obtained with TIP4P. Different curves in the TIP4P results refer to ranges where a different ice nanotube is stable. The melting temperature of bulk water according to our MLP is 270 ± 5 K⁷ and is shown on the plot with a shaded light blue area.

Hence, TIP4P predicts a melting temperature of triangular ice ~ 20 K lower than the bulk, while the TIP4P predicted melting temperatures of square, pentagonal, and hexagonal ice are ~ 30 – 50 K higher than the bulk. In general, the melting point of water is very sensitive to the force-field used to describe the water–water interaction, both in bulk⁷⁴ and under confinement.^{75,76} Reference 76 shows, for instance, a discrepancy of 300 K across empirical forcefields in the predicted melting temperature for 2D water. In addition, we show in the [supplementary material](#) (Sec. S8) that the spectra of bond lengths and angles in the optimized ice nanotubes differ from the fixed value considered in rigid models, a result similar to that found in 2D confinement.⁷ Differences in the bond and angle distribution also influence the charge distributions of the considered systems. In particular, by computing the Wannier centers with DFT (revPBE0-D3) at zero temperature, we estimate an average dipole moment $\mu \sim 2.7$ D for each ice nanotube, as opposed to $D \sim 2.18$ D for TIP4P.⁷⁷ It has been shown that small differences in the multipole moments of a water model can result in ~ 100 K changes in the bulk melting temperature.⁷⁷ Although our analysis is qualitative, this might help explain the differences between TIP4P and our MLP. Overall, this analysis emphasizes the need for achieving predictive ability with first principles accuracy and suggests that our work provides valuable insight into the phase diagram of nano-confined ice.

B. Continuous or discontinuous phase transition?

The nature of the melting phase transition is of special interest for water under confinement. In fact, while the melting in bulk systems is a first-order direct process, in low dimensional systems it can be more complex. For instance, 2D ice has been predicted to melt into a liquid via a hexatic phase.^{7,78} The order of phase transitions resembles a first order for solid to hexatic, but a second order for hexatic to liquid.⁷ In the case of CNTs, previous empirical force-field MD studies showed that water in carbon nanotubes may freeze either continuously or discontinuously, with strong sensitivity to diameter and pressure.^{11,18,41} In particular, at ambient pressure, TIP4P simulations from Ref. 11 suggest that the melting transition is continuous for pores with diameters $d > 12$ Å, while it can be both continuous or discontinuous for $d < 12$ Å. In contrast, ReaxFF simulations from Ref. 18 suggest that the phase transition is discontinuous for hexagonal ice and continuous for square and pentagonal ice, while triangular ice undergoes a supercritical transition with the absence of a diffusive regime at high temperatures. Indeed, it has been shown for 2D nano-capillaries that the order of solid–liquid phase transitions of empirical forcefields is sensitive to their parameterization.⁷⁶

In Fig. 2, we report the density (a) and the diffusion coefficient D_z along the nanotube axis (b) as a function of temperature.

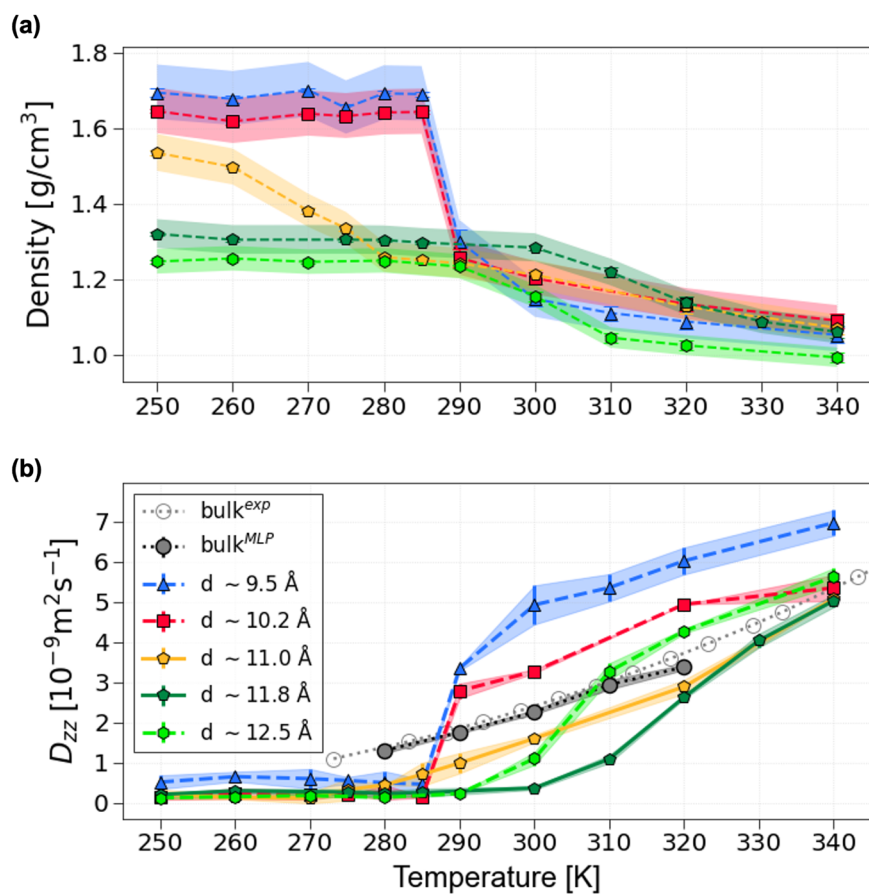


FIG. 2. Melting phase transition of nano-confined ice tubes. We report the density [panel (a)] and the diffusion coefficient D_z along the cylinder axis [panel (b)] as a function of temperature. In panel (b), we also report the diffusion coefficient of bulk water computed with our MLP and compared to experimental results.⁷⁹ Both the density and the diffusion coefficient show signs of a discontinuous phase transition for triangular and square ice and a continuous phase transition for pentagonal and hexagonal ice.

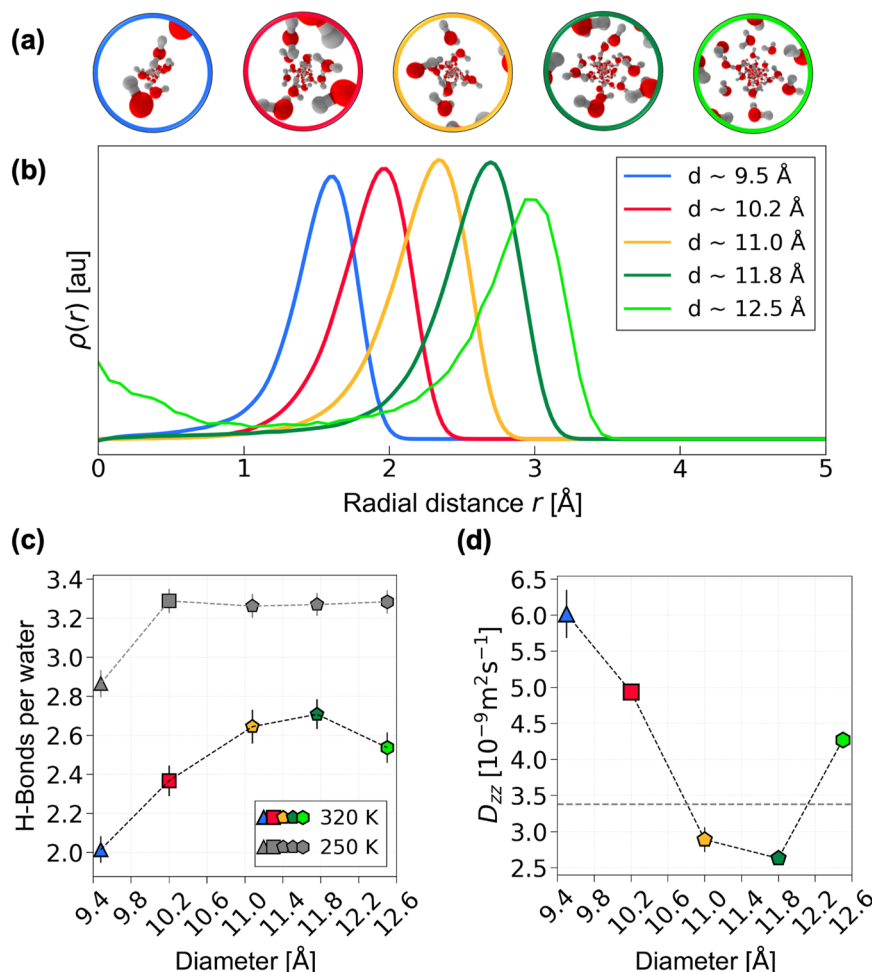


FIG. 3. Structural and dynamical properties of liquid water for different confining diameters at $T = 320$ K. (a) Snapshots of the liquid structures. (b) Radial density $\rho(r)$ as a function of the radial distance r . (c) Average number of hydrogen bonds per water molecule as a function of the nanotube diameter at $T = 250$ K (gray) and $T = 320$ K (blue, red, orange, light, and dark green). (d) Diffusion coefficient D_z along the nanotube axis as a function of the diameter for $T = 320$ K. The bulk value at the same temperature computed with our model is reported with a black dashed line. Increasing the confinement to a diameter $d < 12$ Å results in a more centered liquid with a decreasing number of hydrogen bonds and a corresponding increase in the diffusion coefficient.

We also report the diffusion coefficient of bulk water computed with the MLP and compared to experimental results,⁷⁹ showing the accuracy of our model with quantitative agreement from 280 to 320 K. Details on the calculation of density and the diffusion coefficient are given in Sec. II and in the [supplementary material](#) (Secs. S4 and S5). With our model, both structure (density) and dynamics (diffusion) suggest that the phase transition can be either continuous or discontinuous. In particular, we observe the hallmarks of a discontinuous phase transition for triangular and square ice (stronger confinement regime). On the other hand, seemingly smooth changes in the density and the diffusion coefficient indicate a continuous phase transition for pentagonal and hexagonal ice. As the melting temperature and the order of phase transitions are sensitive to finite size effects, we show in the [supplementary material](#) (Sec. S7) that our results converge with respect to the system size. Overall, such contrasting melting behavior observed within such a narrow range of diameters is a clear illustration of the delicate and fascinating behavior of nano-confined water.

C. Structure and dynamics of nano-confined water depend non-monotonically on the nanotube diameter

So far we focused on identifying the melting temperatures of nano-confined ice tubes. To gain further insight into these systems and to try to understand our observations, we now look at the properties of the liquid as a function of the confinement diameter. In [Fig. 3](#), we report an analysis of the structure and dynamics of the liquid equilibrated at the temperature $T = 320$ K. In particular, we compute the density as a function of the radial distance in the confining cylinder, the average number of hydrogen bonds via geometrical criteria defined in [Ref. 80](#), and the water diffusion coefficient using the velocity autocorrelation function (VACF) method.⁵² We observe a non-monotonic behavior of the average number of hydrogen bonds per molecule as a function of the confining diameter that correlates positively with the non-monotonic trend in the diffusion coefficient.

Increasing the diameter from 9.5 to 11.8 Å results in a less centered liquid, with the peak of the radial density as a function of

the distance from the center r [panel (b)] shifting from $r \sim 1.5$ Å to $r \sim 2.6$ Å. This change is accompanied by an increase in the average number of hydrogen bonds [panel (c)] from ~ 2.0 to ~ 2.7 . The number of hydrogen bonds in the smallest diameter is consistent with both our RSS and previous results¹¹ because only centered chains of water molecules are expected to be stable for $d < 9$ Å. The liquid structure in the largest diameter (12.5 Å) consists of a chain of water molecules inside water rings, in agreement with previous observations.^{11,14,41} This results in a peak in the radial density close to $r \sim 0$ and correlates with a decrease in the number of hydrogen bonds. For comparison, in panel (b), we also show the average number of hydrogen bonds in the solid phases at the temperature $T = 250$ K. The average number of hydrogen bonds in the solid phase shows less sensitivity to the diameter, and it is ~ 3.3 for $d > 10.2$ Å. The number of hydrogen bonds is slightly lower for the triangular phase ($d \sim 9.4$ Å), which is expected due to the helical geometry. The liquid phase diffusion coefficient D_{zz} [panel (d)] shows a consistent trend with the number of hydrogen bonds, increasing from $\sim 3.0 \times 10^{-9}$ m² s⁻¹ at 11.8 Å to $\sim 5.5 \times 10^{-9}$ m² s⁻¹ at 9.4 Å. In particular, the diffusion coefficient for $d < 10$ Å is higher than the bulk value at the same temperature, which is $\sim 3.8 \times 10^{-9}$ m² s⁻¹ with our model. The increase in the diffusion coefficient with stronger confinement is consistent with recent experiments¹⁷ reporting ultra-fast transport (a slip length of ~ 8.5 μm) in vertically aligned CNT membranes with $d < 9$ Å. Qualitatively similar behavior was found with TIP4P/2005 and SPC/E, but not with other empirical force-field simulations, predicting a diffusion coefficient increasing with an increasing diameter in the sub-nanometer regime.^{14,18,81,82}

In summary, we observe that a different liquid is associated with a different confining diameter and ice nanotube, with the melting temperatures varying in a relatively narrow range of ~ 30 K. As the melting temperature depends on the relative Gibbs free energy between a solid and the liquid, we think that the seemingly weak radius dependence of the melting temperature could arise from an overall cancellation of the effects of confinement in both the solid and liquid phases. Finally, we acknowledge that the exact values of both structural and dynamical properties of confined water are expected to be influenced by the modeling of the confining material. However, in the [supplementary material](#) (Sec. S6), we show that our results are consistent with respect to the modeling of explicit CNTs. In fact, we report on the diffusion coefficient and the average number of hydrogen bonds in the three largest nanotubes considered in this work and show results that are in qualitative agreement with those reported in the main paper with the uniform confining potential.

IV. CONCLUSIONS

In this work, we computed the melting temperatures of quasi-one-dimensional ice nanotubes with first principles accuracy. This topic has been debated in the last decades, with both experiments and classical simulations reporting melting temperatures ranging from ~ 180 to ~ 450 K. Exploiting machine learning based first principles accuracy simulations, we show that one-dimensional nanoconfined water is liquid around room temperature. In particular, we computed the melting temperature of (helical) triangular, square, pentagonal, and hexagonal ice in a cylindrical confining potential,

respectively, of diameters $d \sim 9.5, 10.2, 11.0, 11.8,$ and 12.5 Å. We find that all the considered ice nanotubes melt in the range of ~ 280 – 310 K. Our melting temperature of square ice is in agreement with PL spectroscopy experiments;³² similarly, the melting temperatures of pentagonal and hexagonal ice are in agreement with Raman, XRD, and PL spectroscopy experiments.^{22,23,32,33} In addition, the melting temperature of triangular ice is predicted to be higher than previously reported. Notably, empirical force-field simulations predicted melting temperatures differing by as much as ~ 80 K from our MLP, as well as qualitatively different behavior in the diffusion coefficient. We acknowledge that the melting temperature might be sensitive to the reference DFT approximation used to train the MLP, as recently shown for bulk water.⁸³ Therefore, future work might investigate the sensitivity to the reference DFT functional of the melting behavior in one-dimensional confinement. Finally, we provide an insight into the structural and dynamical properties of water confined in different confinement regimes. In a sub-nanoscale confinement regime ($d < 10$ Å), we report a strong reduction in the number of hydrogen bonds and a corresponding enhanced diffusion coefficient that exceeds the bulk limit.

Our model is certainly limited in capturing the effects of chirality and phonon-coupling of the CNTs due to the use of a uniform confining potential. However, we show that the uniform confining potential remains a good model for studying the phase behavior of quasi-1D water. In addition, by changing the confining potential, our simplified model could easily be adapted to the study of different confinement configurations, such as 2D slits of different widths, nanotubes of different diameters, or conical confinement configurations.

In summary, this work suggests that first principles accuracy is required for the modeling of one-dimensional nanoconfined water. In addition, it improves the understanding of the melting transition and structural and dynamical properties of nanoconfined water, providing further insight into technological applications for water filtration and desalination or in the development of artificial channels mimicking biological systems.

SUPPLEMENTARY MATERIAL

See the [supplementary material](#) for details on the CNTs confining potential, validation of our model with diffusion Monte Carlo, the analysis of the coexistence simulations, tests on the estimates of the diffusion coefficient, and comparison between predictions of the implicit and explicit carbon models. See the [supplementary material](#) for details on the CNTs confining potential, validation of our model with diffusion Monte Carlo, the analysis of the coexistence simulations, tests on the estimates of the diffusion coefficient, and comparison between predictions of the implicit and explicit carbon models. The [supplementary material](#) includes Refs. 32, 36, 42, 45, 52, 58–61, 68, and 69.

ACKNOWLEDGMENTS

We thank all members of the ICE group for the valuable feedback on the early stages of the manuscript. We acknowledge

the computational resources from Cambridge Service for Data Driven Discovery (CSD3) operated by the University of Cambridge Research Computing Service (www.csd3.cam.ac.uk), provided by Dell EMC and Intel using Tier-2 funding from the Engineering and Physical Sciences Research Council (capital Grant Nos. EP/T022159/1 and EP/P020259/1), and DiRAC funding from the Science and Technology Facilities Council (www.dirac.ac.uk). We are further grateful for the computational support from the UK national high performance computing service, ARCHER2, for which access was obtained via the UKCP consortium and funded by EPSRC grant ref EP/X035891/1 and the Swiss National Supercomputing Center under project s1209. V.K. acknowledges the support from the Ernest Oppenheimer Early Career Fellowship and the Sydney Harvey Junior Research Fellowship. A.M. acknowledges the support from the European Union under the “n-AQUA” European Research Council project (Grant No. 101071937). D.A. and A.Z. acknowledge the support from Leverhulme Grant No. RPG-2020-038 and from the European Union under the Next Generation EU (Project Nos. 20222FXZ33 and P2022MC742).

AUTHOR DECLARATIONS

Conflict of Interest

The authors have no conflicts to disclose.

Author Contributions

Flaviano Della Pia: Conceptualization (equal); Data curation (equal); Formal analysis (equal); Investigation (equal); Writing – original draft (equal); Writing – review & editing (equal). **Andrea Zen:** Conceptualization (equal); Data curation (equal); Formal analysis (equal); Funding acquisition (equal); Supervision (equal); Writing – review & editing (equal). **Venkat Kapil:** Conceptualization (equal); Data curation (equal); Formal analysis (equal); Resources (equal); Supervision (equal); Writing – review & editing (equal). **Fabian L. Thiemann:** Conceptualization (equal); Data curation (equal); Formal analysis (equal); Supervision (equal); Writing – review & editing (equal). **Dario Alfè:** Conceptualization (equal); Data curation (equal); Formal analysis (equal); Funding acquisition (equal); Project administration (equal); Resources (equal); Supervision (equal); Writing – review & editing (equal). **Angeles Michaelides:** Conceptualization (equal); Data curation (equal); Formal analysis (equal); Funding acquisition (equal); Project administration (equal); Resources (equal); Supervision (equal); Writing – review & editing (equal).

DATA AVAILABILITY

The data that support the findings of this study are available within the article and its [supplementary material](#). Additional scripts and input files necessary to reproduce the findings of this work are available on [GitHub](#).

REFERENCES

¹L. Fumagalli, A. Esfandiari, R. Fabregas, S. Hu, P. Ares, A. Janardanan, Q. Yang, B. Radha, T. Taniguchi, K. Watanabe, G. Gomila, K. S. Novoselov, and A. K. Geim,

“Anomalously low dielectric constant of confined water,” *Science* **360**, 1339–1342 (2018).

²A. I. Kolesnikov, J.-M. Zanotti, C.-K. Loong, P. Thiyagarajan, A. P. Moravsky, R. O. Loutfy, and C. J. Burnham, “Anomalously soft dynamics of water in a nanotube: A revelation of nanoscale confinement,” *Phys. Rev. Lett.* **93**, 035503 (2004).

³E. Secchi, S. Marbach, A. Niguès, D. Stein, A. Siria, and L. Bocquet, “Massive radius-dependent flow slippage in carbon nanotubes,” *Nature* **537**, 210 (2016).

⁴N. Kavokine, M.-L. Bocquet, and L. Bocquet, “Fluctuation-induced quantum friction in nanoscale water flows,” *Nature* **602**, 84 (2022).

⁵A. T. Bui, F. L. Thiemann, A. Michaelides, and S. J. Cox, “Classical quantum friction at water–carbon interfaces,” *Nano Lett.* **23**, 580–587 (2023).

⁶N. Kastelowitz and V. Molinero, “Ice–liquid oscillations in nanoconfined water,” *ACS Nano* **12**, 8234–8239 (2018).

⁷V. Kapil, C. Schran, A. Zen, J. Chen, C. J. Pickard, and A. Michaelides, “The first-principles phase diagram of monolayer nanoconfined water,” *Nature* **609**, 512–516 (2022).

⁸S. P. Surwade, S. N. Smirnov, I. V. Vlassiok, R. R. Unocic, G. M. Veith, S. Dai, and S. M. Mahurin, “Water desalination using nanoporous single-layer graphene,” *Nat. Nanotechnol.* **10**, 459 (2015).

⁹H. G. Park and Y. Jung, “Carbon nanofluidics of rapid water transport for energy applications,” *Chem. Soc. Rev.* **43**, 565–576 (2014).

¹⁰Z. Zhang, L. Wen, and L. Jiang, “Nanofluidics for osmotic energy conversion,” *Nat. Rev. Mater.* **6**, 622 (2021).

¹¹D. Takaiwa, I. Hatano, K. Koga, and H. Tanaka, “Phase diagram of water in carbon nanotubes,” *Proc. Natl. Acad. Sci. U. S. A.* **105**, 39 (2008).

¹²K. Mochizuki and K. Koga, “Solid–liquid critical behavior of water in nanopores,” *Proc. Natl. Acad. Sci. U. S. A.* **112**, 8221–8226 (2015).

¹³J. Köfinger, G. Hummer, and C. Dellago, “Macroscopically ordered water in nanopores,” *Proc. Natl. Acad. Sci. U. S. A.* **105**, 13218–13222 (2008).

¹⁴A. Barati Farimani and N. R. Aluru, “Spatial diffusion of water in carbon nanotubes: From fickian to ballistic motion,” *J. Phys. Chem. B* **115**, 12145–12149 (2011).

¹⁵A. Striolo, “The mechanism of water diffusion in narrow carbon nanotubes,” *Nano Lett.* **6**, 633–639 (2006).

¹⁶J. K. Holt, H. G. Park, Y. Wang, M. Stadermann, A. B. Artyukhin, C. P. Grigoropoulos, A. Noy, and O. Bakajin, “Fast mass transport through sub-2-nanometer carbon nanotubes,” *Science* **312**, 1034–1037 (2006).

¹⁷D.-C. Yang, R. J. Castellano, R. P. Silvy, S. K. Lageshetty, R. F. Praino, F. Fornasiero, and J. W. Shan, “Fast water transport through subnanometer diameter vertically aligned carbon nanotube membranes,” *Nano Lett.* **23**, 4956–4964 (2023).

¹⁸M. Raju, A. van Duin, and M. Ihme, “Phase transitions of ordered ice in graphene nanocapillaries and carbon nanotubes,” *Sci. Rep.* **8**, 3851 (2018).

¹⁹K. Mochizuki, Y. Adachi, and K. Koga, “Close-packed ices in nanopores,” *ACS Nano* **18**, 347–354 (2024).

²⁰D. Wang, N. B. Saleh, W. Sun, C. M. Park, C. Shen, N. Aich, W. J. G. M. Peijnenburg, W. Zhang, Y. Jin, and C. Su, “Next-generation multifunctional carbon–metal nanohybrids for energy and environmental applications,” *Environ. Sci. Technol.* **53**, 7265–7287 (2019).

²¹X. Fan, G. Wei, and X. Quan, “Carbon nanomaterial-based membranes for water and wastewater treatment under electrochemical assistance,” *Environ. Sci.: Nano* **10**, 11–40 (2023).

²²Y. Maniwa, H. Kataura, M. Abe, A. Uda, S. Suzuki, Y. Achiba, H. Kira, K. Matsuda, H. Kadowaki, and Y. Okabe, “Ordered water inside carbon nanotubes: Formation of pentagonal to octagonal ice-nanotubes,” *Chem. Phys. Lett.* **401**, 534–538 (2005).

²³H. Kyakuno, K. Matsuda, H. Yahiro, Y. Inami, T. Fukuoka, Y. Miyata, K. Yanagi, Y. Maniwa, H. Kataura, T. Saito, M. Yumura, and S. Iijima, “Confined water inside single-walled carbon nanotubes: Global phase diagram and effect of finite length,” *J. Chem. Phys.* **134**, 244501 (2011).

²⁴J. Shiomi, T. Kimura, and S. Maruyama, “Molecular dynamics of ice-nanotube formation inside carbon nanotubes,” *J. Phys. Chem. C* **111**, 12188–12193 (2007).

²⁵F. Mikami, K. Matsuda, H. Kataura, and Y. Maniwa, “Dielectric properties of water inside single-walled carbon nanotubes,” *ACS Nano* **3**, 1279–1287 (2009).

²⁶C. Luo, W. Fa, J. Zhou, J. Dong, and X. C. Zeng, “Ferroelectric ordering in ice nanotubes confined in carbon nanotubes,” *Nano Lett.* **8**, 2607–2612 (2008).

- ²⁷J. H. Walther, K. Ritos, E. R. Cruz-Chu, C. M. Megaridis, and P. Koumoutsakos, “Barriers to superfast water transport in carbon nanotube membranes,” *Nano Lett.* **13**, 1910–1914 (2013).
- ²⁸S. Ghosh, A. K. Sood, and N. Kumar, “Carbon nanotube flow sensors,” *Science* **299**, 1042–1044 (2003).
- ²⁹M. Majumder, A. Stinchcomb, and B. J. Hinds, “Towards mimicking natural protein channels with aligned carbon nanotube membranes for active drug delivery,” *Life Sci.* **86**, 563–568 (2010).
- ³⁰F. Zhu and K. Schulten, “Water and proton conduction through carbon nanotubes as models for biological channels,” *Biophys. J.* **85**, 236–244 (2003).
- ³¹R. H. Tunuguntla, R. Y. Henley, Y.-C. Yao, T. A. Pham, M. Wanunu, and A. Noy, “Enhanced water permeability and tunable ion selectivity in subnanometer carbon nanotube porins,” *Science* **357**, 792–796 (2017).
- ³²S. Chiashi, Y. Saito, T. Kato, S. Konabe, S. Okada, T. Yamamoto, and Y. Homma, “Confinement effect of sub-nanometer difference on melting point of ice-nanotubes measured by photoluminescence spectroscopy,” *ACS Nano* **13**, 1177 (2019).
- ³³K. V. Agrawal, S. Shimizu, L. W. Draughshuk, D. Kilcoyne, and M. S. Strano, “Observation of extreme phase transition temperatures of water confined inside isolated carbon nanotubes,” *Nat. Nanotechnol.* **12**, 267 (2017).
- ³⁴M. Perez, “Gibbs–Thomson effects in phase transformations,” *Scr. Mater.* **52**, 709–712 (2005).
- ³⁵H. K. Christenson, “Confinement effects on freezing and melting,” *J. Phys.: Condens. Matter* **13**, R95 (2001).
- ³⁶W. L. Jorgensen, J. Chandrasekhar, J. D. Madura, R. W. Impey, and M. L. Klein, “Comparison of simple potential functions for simulating liquid water,” *J. Chem. Phys.* **79**, 926–935 (1983).
- ³⁷H. J. C. Berendsen, J. R. Grigera, and T. P. Straatsma, “The missing term in effective pair potentials,” *J. Phys. Chem.* **91**, 6269–6271 (1987).
- ³⁸A. C. T. van Duin, S. Dasgupta, F. Lorant, and W. A. Goddard, “ReaxFF: A reactive force field for hydrocarbons,” *J. Phys. Chem. A* **105**, 9396–9409 (2001).
- ³⁹J. Behler, “Four generations of high-dimensional neural network potentials,” *Chem. Rev.* **121**, 10037–10072 (2021).
- ⁴⁰A. Omranpour, P. Montero De Hijas, J. Behler, and C. Dellago, “Perspective: Atomistic simulations of water and aqueous systems with machine learning potentials,” *J. Chem. Phys.* **160**, 170901 (2024).
- ⁴¹K. Koga, G. T. Gao, H. Tanaka, and X. C. Zeng, “Formation of ordered ice nanotubes inside carbon nanotubes,” *Nature* **412**, 802–805 (2001).
- ⁴²F. L. Thiemann, C. Schran, P. Rowe, E. A. Müller, and A. Michaelides, “Water flow in single-wall nanotubes: Oxygen makes it slip, hydrogen makes it stick,” *ACS Nano* **16**, 10775–10782 (2022).
- ⁴³C. J. Pickard and R. J. Needs, “*Ab initio* random structure searching,” *J. Phys.: Condens. Matter* **23**, 053201 (2011).
- ⁴⁴P. Ravindra, X. R. Advincula, C. Schran, A. Michaelides, and V. Kapil, “Quasi-one-dimensional hydrogen bonding in nanoconfined ice,” *Nat. Commun.* **15**, 7301 (2024).
- ⁴⁵J. G. Brandenburg, A. Zen, D. Alfè, and A. Michaelides, “Interaction between water and carbon nanostructures: How good are current density functional approximations?,” *J. Chem. Phys.* **151**, 164702 (2019).
- ⁴⁶C. Schran, K. Brezina, and O. Marsalek, “Committee neural network potentials control generalization errors and enable active learning,” *J. Chem. Phys.* **153**, 104105 (2020).
- ⁴⁷C. Schran, F. L. Thiemann, P. Rowe, E. A. Müller, O. Marsalek, and A. Michaelides, “Machine learning potentials for complex aqueous systems made simple,” *Proc. Natl. Acad. Sci. U. S. A.* **118**, e2110077118 (2021).
- ⁴⁸M. M. Conde, M. Rovere, and P. Gallo, “High precision determination of the melting points of water TIP4P/2005 and water TIP4P/Ice models by the direct coexistence technique,” *J. Chem. Phys.* **147**, 244506 (2017).
- ⁴⁹R. García Fernández, J. L. F. Abascal, and C. Vega, “The melting point of ice Ih for common water models calculated from direct coexistence of the solid–liquid interface,” *J. Chem. Phys.* **124**, 144506 (2006).
- ⁵⁰D. Alfè, “First-principles simulations of direct coexistence of solid and liquid aluminum,” *Phys. Rev. B* **68**, 064423 (2003).
- ⁵¹D. Alfè, “Temperature of the inner-core boundary of the earth: Melting of iron at high pressure from first-principles coexistence simulations,” *Phys. Rev. B* **79**, 060101 (2009).
- ⁵²D. Frenkel and B. Smit, *Understanding Molecular Simulation: From Algorithms to Applications* (Elsevier, 2023).
- ⁵³I.-C. Yeh and G. Hummer, “System-size dependence of diffusion coefficients and viscosities from molecular dynamics simulations with periodic boundary conditions,” *J. Phys. Chem. B* **108**, 15873–15879 (2004).
- ⁵⁴V. Kapil, M. Rossi, O. Marsalek, R. Petraglia, Y. Litman, T. Spura, B. Cheng, A. Cuzzocrea, R. H. Meißner, D. M. Wilkins, B. A. Helfrecht, P. Juda, S. P. Bienvenue, W. Fang, J. Kessler, I. Poltavsky, S. Vandenbrande, J. Wieme, C. Corminboeuf, T. D. Kühne, D. E. Manolopoulos, T. E. Markland, J. O. Richardson, A. Tkatchenko, G. A. Tribello, V. Van Speybroeck, and M. Ceriotti, “i-PI 2.0: A universal force engine for advanced molecular simulations,” *Comput. Phys. Commun.* **236**, 214–223 (2019).
- ⁵⁵A. Singraber, J. Behler, and C. Dellago, “Library-based LAMMPS implementation of high-dimensional neural network potentials,” *J. Chem. Theory Comput.* **15**, 1827–1840 (2019).
- ⁵⁶A. P. Thompson, H. M. Aktulga, R. Berger, D. S. Bolintineanu, W. M. Brown, P. S. Crozier, P. J. in ’t Veld, A. Kohlmeyer, S. G. Moore, T. D. Nguyen, R. Shan, M. J. Stevens, J. Tranchida, C. Trit, and S. J. Plimpton, “LAMMPS—A flexible simulation tool for particle-based materials modeling at the atomic, meso, and continuum scales,” *Comput. Phys. Commun.* **271**, 108171 (2022).
- ⁵⁷A. Hjorth Larsen, J. Jørgen Mortensen, J. Blomqvist, I. E. Castelli, R. Christensen, M. Dulak, J. Friis, M. N. Groves, B. Hammer, C. Hargus, E. D. Hermes, P. C. Jennings, P. Bjerre Jensen, J. Kermode, J. R. Kitchin, E. Leonhard Kolsbjerg, J. Kubal, K. Kaasbjerg, S. Lygaard, J. Bergmann Maronsson, T. Maxson, T. Olsen, L. Pastewka, A. Peterson, C. Rostgaard, J. Schiøtz, O. Schütt, M. Strange, K. S. Thygesen, T. Vegge, L. Vilhelmsen, M. Walter, Z. Zeng, and K. W. Jacobsen, “The atomic simulation environment—A Python library for working with atoms,” *J. Phys.: Condens. Matter* **29**, 273002 (2017).
- ⁵⁸G. Kresse and J. Hafner, “*Ab initio* molecular dynamics for liquid metals,” *Phys. Rev. B* **47**, 558 (1993).
- ⁵⁹G. Kresse and J. Hafner, “*Ab initio* molecular-dynamics simulation of the liquid-metal-amorphous-semiconductor transition in germanium,” *Phys. Rev. B* **49**, 14251 (1994).
- ⁶⁰G. Kresse and J. Furthmüller, “Efficiency of *ab-initio* total energy calculations for metals and semiconductors using a plane-wave basis set,” *Comput. Mater. Sci.* **6**, 15–50 (1996).
- ⁶¹G. Kresse and J. Furthmüller, “Efficient iterative schemes for *ab initio* total-energy calculations using a plane-wave basis set,” *Phys. Rev. B* **54**, 11169 (1996).
- ⁶²R. J. Needs, M. Towler, N. Drummond, P. López Ríos, and J. Trail, “Variational and diffusion quantum Monte Carlo calculations with the CASINO code,” *J. Chem. Phys.* **152**, 154106 (2020).
- ⁶³J. R. Trail and R. J. Needs, “Shape and energy consistent pseudopotentials for correlated electron systems,” *J. Chem. Phys.* **146**, 204107 (2017).
- ⁶⁴A. Zen, J. G. Brandenburg, A. Michaelides, and D. Alfè, “A new scheme for fixed node diffusion quantum Monte Carlo with pseudopotentials: Improving reproducibility and reducing the trial-wave-function bias,” *J. Chem. Phys.* **151**, 134105 (2019).
- ⁶⁵L. Fraser, W. Foulkes, G. Rajagopal, R. Needs, S. Kenny, and A. Williamson, “Finite-size effects and Coulomb interactions in quantum Monte Carlo calculations for homogeneous systems with periodic boundary conditions,” *Phys. Rev. B* **53**, 1814–1832 (1996).
- ⁶⁶A. Williamson, G. Rajagopal, R. Needs, L. Fraser, W. Foulkes, Y. Wang, and M.-Y. Chou, “Elimination of Coulomb finite-size effects in quantum many-body simulations,” *Phys. Rev. B* **55**, R4851 (1997).
- ⁶⁷P. R. C. Kent, R. Q. Hood, A. J. Williamson, R. J. Needs, W. M. C. Foulkes, and G. Rajagopal, “Finite-size errors in quantum many-body simulations of extended systems,” *Phys. Rev. B* **59**, 1917–1929 (1999).
- ⁶⁸A. Zen, S. Sorella, M. J. Gillan, A. Michaelides, and D. Alfè, “Boosting the accuracy and speed of quantum Monte Carlo: Size consistency and time step,” *Phys. Rev. B* **93**, 241118 (2016).

- ⁶⁹F. Della Pia, A. Zen, D. Alfè, and A. Michaelides, “DMC-ICE13: Ambient and high pressure polymorphs of ice from diffusion Monte Carlo and density functional theory,” *J. Chem. Phys.* **157**, 134701 (2022).
- ⁷⁰Y. Zhang and W. Yang, “Comment on ‘Generalized gradient approximation made simple,’” *Phys. Rev. Lett.* **80**, 890 (1998).
- ⁷¹S. Grimme, J. Antony, S. Ehrlich, and H. Krieg, “A consistent and accurate *ab initio* parametrization of density functional dispersion correction (DFT-D) for the 94 elements H-Pu,” *J. Chem. Phys.* **132**, 154104 (2010).
- ⁷²L. Goerigk and S. Grimme, “A thorough benchmark of density functional methods for general main group thermochemistry, kinetics, and noncovalent interactions,” *Phys. Chem. Chem. Phys.* **13**, 6670–6688 (2011).
- ⁷³B. Cheng, E. A. Engel, J. Behler, C. Dellago, and M. Ceriotti, “Ab initio thermodynamics of liquid and solid water,” *Proc. Natl. Acad. Sci. U. S. A.* **116**, 1110–1115 (2019).
- ⁷⁴S. Blazquez and C. Vega, “Melting points of water models: Current situation,” *J. Chem. Phys.* **156**, 216101 (2022).
- ⁷⁵J. Li, C. Zhu, W. Zhao, Y. Gao, J. Bai, J. Jiang, and X. C. Zeng, “Formation of a two-dimensional helical square tube ice in hydrophobic nanoslit using the TIP5P water model,” *J. Chem. Phys.* **160**, 164716 (2024).
- ⁷⁶S. Li and B. Schmidt, “Replica exchange md simulations of two-dimensional water in graphene nanocapillaries: Rhombic versus square structures, proton ordering, and phase transitions,” *Phys. Chem. Chem. Phys.* **21**, 17640–17654 (2019).
- ⁷⁷J. L. F. Abascal and C. Vega, “The water forcefield: Importance of dipolar and quadrupolar interactions,” *J. Phys. Chem. C* **111**, 15811–15822 (2007).
- ⁷⁸J. Zubeltzu, F. Corsetti, M. V. Fernández-Serra, and E. Artacho, “Continuous melting through a hexatic phase in confined bilayer water,” *Phys. Rev. E* **93**, 062137 (2016).
- ⁷⁹M. Holz, S. R. Heil, and A. Sacco, “Temperature-dependent self-diffusion coefficients of water and six selected molecular liquids for calibration in accurate ¹H NMRPFG measurements,” *Phys. Chem. Chem. Phys.* **2**, 4740–4742 (2000).
- ⁸⁰A. Luzar and D. Chandler, “Hydrogen-bond kinetics in liquid water,” *Nature* **379**, 55–57 (1996).
- ⁸¹B. H. S. Mendonça, E. E. de Moraes, R. J. C. Batista, A. B. de Oliveira, M. C. Barbosa, and H. Chacham, “Water diffusion in carbon nanotubes for rigid and flexible models,” *J. Phys. Chem. C* **127**, 9769–9778 (2023).
- ⁸²A. Chatzichristos and J. Hassan, “Current understanding of water properties inside carbon nanotubes,” *Nanomaterials* **12**, 174 (2022).
- ⁸³P. Montero de Hijes, C. Dellago, R. Jinnouchi, and G. Kresse, “Density isobar of water and melting temperature of ice: Assessing common density functionals,” *J. Chem. Phys.* **161**(13), 131102 (2024).